AGU PUBLICATIONS

Geophysical Research Letters

RESEARCH LETTER
10.1002/2016GL069212

Special Section:
First results from NASA's Magnetospheric Multiscale (MMS) Mission

MMS observations of electron-scale filamentary currents in the reconnection exhaust and near the X line

T. D. Phan[1], J. P. Eastwood[2], P. A. Cassak[3], M. Øieroset[1], J. T. Gosling[4], D. J. Gershman[5,6], F. S. Mozer[1], M. A. Shay[7], M. Fujimoto[8], W. Daughton[9], J. F. Drake[10], J. L. Burch[11], R. B. Torbert[11,12], R. E. Ergun[4], L. J. Chen[5,6], S. Wang[6], C. Pollock[13], J. C. Dorelli[5], B. Lavraud[14,15], B. L. Giles[5], T. E. Moore[5], Y. Saito[8], L. A. Avanov[5,6], W. Paterson[5], R. J. Strangeway[16], C. T. Russell[16], Y. Khotyaintsev[17], P. A. Lindqvist[18], M. Oka[1], and F. D. Wilder[4]

[1]Space Sciences Laboratory, University of California, Berkeley, California, USA, [2]The Blackett Laboratory, Imperial College London, London, UK, [3]Department of Physics and Astronomy, West Virginia University, Morgantown, West Virginia, USA, [4]LASP, University of Colorado, Boulder, Colorado, USA, [5]NASA Goddard Space Flight Center, Greenbelt, Maryland, USA, [6]Department of Physics and the Institute for Physical Science and Technology, University of Maryland, College Park, Maryland, USA, [7]Department of Physics and Astronomy, University of Delaware, Newark, Delaware, USA, [8]ISAS/JAXA, Kanagawa, Japan, [9]Los Alamos National Laboratory, Los Alamos, New Mexico, USA, [10]Department of Astronomy, University of Maryland, College Park, Maryland, USA, [11]Southwest Research Institute, San Antonio, Texas, USA, [12]Institute for the Study of Earth, Oceans, and Space, University of New Hampshire, Durham, New Hampshire, USA, [13]Denali Scientific, Healy, Alaska, USA, [14]Institut de Recherche en Astrophysique et Planétologie, Université de Toulouse, Toulouse, France, [15]Centre National de la Recherche Scientifique, Toulouse, France, [16]Department of Earth, Planetary, and Space Sciences, University of California, Los Angeles, California, USA, [17]Swedish Institute of Space Physics, Uppsala, Sweden, [18]Royal Institute of Technology, Stockholm, Sweden

Key Points:
- Demonstrate unprecedented MMS measurements of current density at 30 ms, capable of resolving current layers on electron skin depth scales
- Evidence for electron-scale filamentary Hall currents in exhaust and at its boundaries ~70 ion skin depths downstream of the X line
- Nongyrotropic crescent shape electron distributions in electron current layer embedded in the ion diffusion region near the X line

Supporting Information:
- Text S1

Correspondence to:
T. D. Phan,
phan@ssl.berkeley.edu

Citation:
Phan, T. D., et al. (2016), MMS observations of electron-scale filamentary currents in the reconnection exhaust and near the X line, *Geophys. Res. Lett.*, *43*, 6060–6069, doi:10.1002/2016GL069212.

Received 18 APR 2016
Accepted 3 JUN 2016
Accepted article online 5 JUN 2016
Published online 29 JUN 2016

Abstract We report Magnetospheric Multiscale observations of macroscopic and electron-scale current layers in asymmetric reconnection. By intercomparing plasma, magnetic, and electric field data at multiple crossings of a reconnecting magnetopause on 22 October 2015, when the average interspacecraft separation was ~10 km, we demonstrate that the ion and electron moments are sufficiently accurate to provide reliable current density measurements at 30 ms cadence. These measurements, which resolve current layers narrower than the interspacecraft separation, reveal electron-scale filamentary Hall currents and electron vorticity within the reconnection exhaust far downstream of the X line and even in the magnetosheath. Slightly downstream of the X line, intense (up to 3 $\mu A/m^2$) electron currents, a super-Alfvénic outflowing electron jet, and nongyrotropic crescent shape electron distributions were observed deep inside the ion-scale magnetopause current sheet and embedded in the ion diffusion region. These characteristics are similar to those attributed to the electron dissipation/diffusion region around the X line.

1. Introduction

The ability to accurately measure current density is crucial for understanding the magnetic reconnection process as it reveals both the structure of the macroscopic current systems and small-scale structure of dissipation regions. Theory and kinetic simulations [e.g., *Sonnerup*, 1979] predict that the structure of the macroscopic current systems strongly depends on boundary conditions such as the size of the guide field [e.g., *Swisdak et al.*, 2005], the level of asymmetry on the two sides of the current sheet [e.g., *Krauss-Varban et al.*, 1999], and the presence of flow shears [e.g., *Tanaka et al.*, 2010]. Furthermore, some work suggests that 3-D simulations generate more electron-scale current sheets than 2-D simulations. One particular manifestation of this possible 3-D effect is the occurrence of highly filamentary current sheets within the exhaust, in addition to the breakup of intense currents along the separatrices [*Daughton et al.*, 2011; *Che et al.*, 2011].

Experimental analysis of the current density directly determined from plasma measurements is difficult due to the usually large uncertainties in the electron velocity measurements. When appropriate multipoint magnetic field measurements are available, the current density can be computed via the curlometer method [*Robert et al.*, 1998; *Dunlop et al.*, 2002]. However, this method is only valid when the scale size of the spacecraft tetrahedron configuration is much less than the structure under consideration and the current density is approximately uniform on the spacecraft separation scale. Cluster data obtained when the tetrahedron scale

was 100 km were used to calculate current density at the magnetopause [*Dunlop et al.*, 2002], but was unable to explore current densities at scale sizes below 100 km.

In this paper, we first demonstrate that the Magnetospheric Multiscale (MMS) ion and electron measurements are sufficiently accurate to provide reliable single-spacecraft current density measurements at 30 ms cadence (or 1.3 electron skin depth resolution). This analysis uses burst-mode data from the fluxgate magnetometer at 128 samples per second [*Russell et al.*, 2014], the fast plasma experiment at 150 ms resolution for ions and 30 ms resolution for electrons [*Pollock et al.*, 2016], and the electric field instrument at 8192 samples/s [*Torbert et al.*, 2014]. We then use these current density measurements, made independently by each of the four MMS satellites in a 10 km scale tetrahedron configuration, to reveal and explore for the first time electron-scale filamentary currents both near the X line and in the downstream exhaust.

2. Overview

Figure 1 shows an overview of multiple crossings of a dayside (13.5 magnetic local time) magnetopause reconnection layer by MMS 1. This interval was chosen because the spacecraft encountered both the exhaust (~70 ion skin depths (d_i) downstream of the X line) and the region around the X line. During this interval the average separation of the four spacecraft was ~10 km, or ~8 electron skin depths (d_e) based on the magnetosheath density of ~25 cm^{-3}. The data are shown in *LMN* boundary normal coordinates determined by minimum variance analysis [*Sonnerup and Cahill*, 1967] of the complete magnetopause crossing at 06:03:54–06:04:09 UT and assumed to be the same for the rest of the interval shown. *N* is along the magnetopause normal, *L* is along the reconnecting field direction, and *M* points approximately along the X line.

Initially, MMS 1 was in the magnetosheath where the magnetic field (Figure 1a) pointed southward ($B_L < 0$) and the plasma density (Figure 1d) was ~25 cm^{-3}. From 06:03:54 to 06:04:08 UT (marked by the two vertical dashed lines), the spacecraft crossed the magnetopause current sheet into the magnetosphere where the magnetic field pointed northward ($B_L > 0$) and the number density was ~4 cm^{-3}. The number density was unusually high in the magnetosphere because of the presence of cold plasma (see Figure 1m). Embedded in the magnetopause was a southward directed ion jet (Figure 1e) reaching nearly −155 km/s (relative to the magnetosheath $V_L \sim -40$ km/s, marked by the horizontal black dashed line), or approximately 90% of the magnetosheath (inflow) Alfven speed of ~175 km/s. This indicates that MMS 1 encountered a reconnection exhaust south of the X line. Interpenetrating magnetosheath and magnetospheric ion beams in the jet (Figures 1l and 1m), as well as reflected magnetosheath ions detected in the magnetosheath (Figure 1k), provide further evidence for reconnection. The magnetic field rotation across the magnetopause was ~175°. A large out-of-plane magnetic field (B_M) was present in the exhaust with amplitude of 48 nT, which was larger than B_L in the magnetosheath. Large B_M in the exhaust does not imply that the spacecraft was close to the X line because, as shown below, this exhaust encounter occurred far downstream of the X line. More interestingly, the sign of B_M was not consistent with a Hall field south of the X line [e.g., *Tanaka et al.*, 2008]. This discrepancy will be discussed in section 5.

Four-spacecraft timing analysis (not shown) reveals that the magnetopause normal motion at 06:04 UT was outward at ~44 km/s. The current sheet width was thus ~645 km, or 14 magnetosheath d_i. Assuming a reconnection rate of 0.1 (thus an exhaust opening angle of 11°), this exhaust crossing occurred ~70 d_i downstream of the X line.

At 06:05:06 UT, MMS 1 re-entered the reconnecting magnetopause, still south of the X line as evidenced by the presence of a southward ion jet ($V_L < 0$). A bit later, at ~06:05:20 UT, MMS 1 detected a V_L reversal. This suggests that the spacecraft was in close proximity of the X line at that time.

There were noticeable differences between the reconnection exhaust at 06:03:54–06:04:08 UT and the broad region (06:05:05–06:05:30 UT) surrounding the flow reversal. The electron temperature in the flow reversal interval was much higher than in the earlier exhaust (Figure 1h), and the currents (Figures 1i and 1j) were more intense, with peak amplitudes reaching 3 $\mu A/m^2$. Two measures of the current density, $\mathbf{j}_P = ne(\mathbf{V}_i\text{-}\mathbf{V}_e)$ based on the plasma measurements, and $\mathbf{j}_B = \nabla \times \mathbf{B}/\mu_0$ based on the curlometer method, are shown in Figures 1i and 1j, respectively. There is general agreement between the two measurements on large scales, but on smaller scales, the amplitudes of $\mathbf{j}_P$ are larger than $\mathbf{j}_B$. In the next section we will demonstrate the accuracy of $\mathbf{j}_P$ and show the common occurrence of filamentary currents with scale sizes below the 10 km spacecraft separation. For such currents, the curlometer method underestimates the current density.

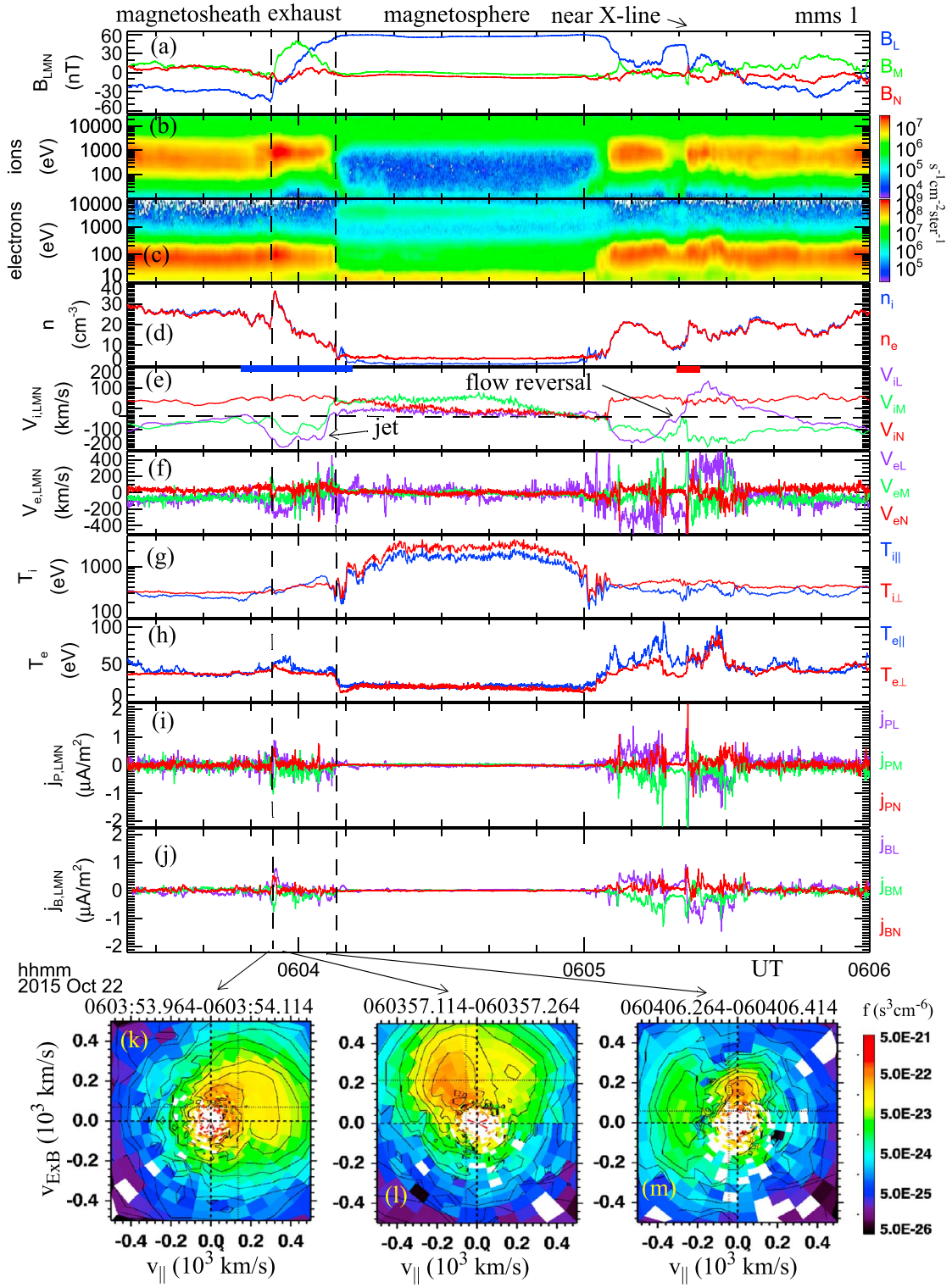

Figure 1. MMS 1 multiple crossings of a reconnecting magnetopause on 22 Oct 2015 in *LMN* coordinates. (a) Magnetic field, (b and c) ion and electron spectrograms of energy flux, (d) ion and electron densities, (e and f) ion and electron velocities, (g and h) ion and electron temperatures, (i) current computed from ne($\mathbf{V}_i$-$\mathbf{V}_e$), (j) current computed from $\nabla \times \mathbf{B}/\mu_0$, and (k–m) 2-D cuts of 3-D ion distributions in the spacecraft frame in the plane that contains the magnetic field and $\mathbf{E} \times \mathbf{B}$ directions, where $\mathbf{E}$ was obtained from $-\mathbf{v} \times \mathbf{B}$. In the distribution shown in Figure 1k the field-aligned velocity separation between the incident and reflected magnetosheath ions was ~220 km/s, close to the predicted 2 V_{HT} [*Cowley*, 1982; *Fuselier et al.*, 1990; *Gosling et al.*, 1991], where V_{HT} is the deHoffman-Teller speed (which is 125 km/s for the exhaust interval). The *LMN* coordinates: $L = (0.42, -0.53, 0.91)_{GSE}$, $M = (0.64, -0.70, -0.33)_{GSE}$, $N = (0.65, 0.72, -0.26)_{GSE}$. Ion moments in the magnetosphere are not reliable due to the 10 eV lower limit of the plasma instruments.

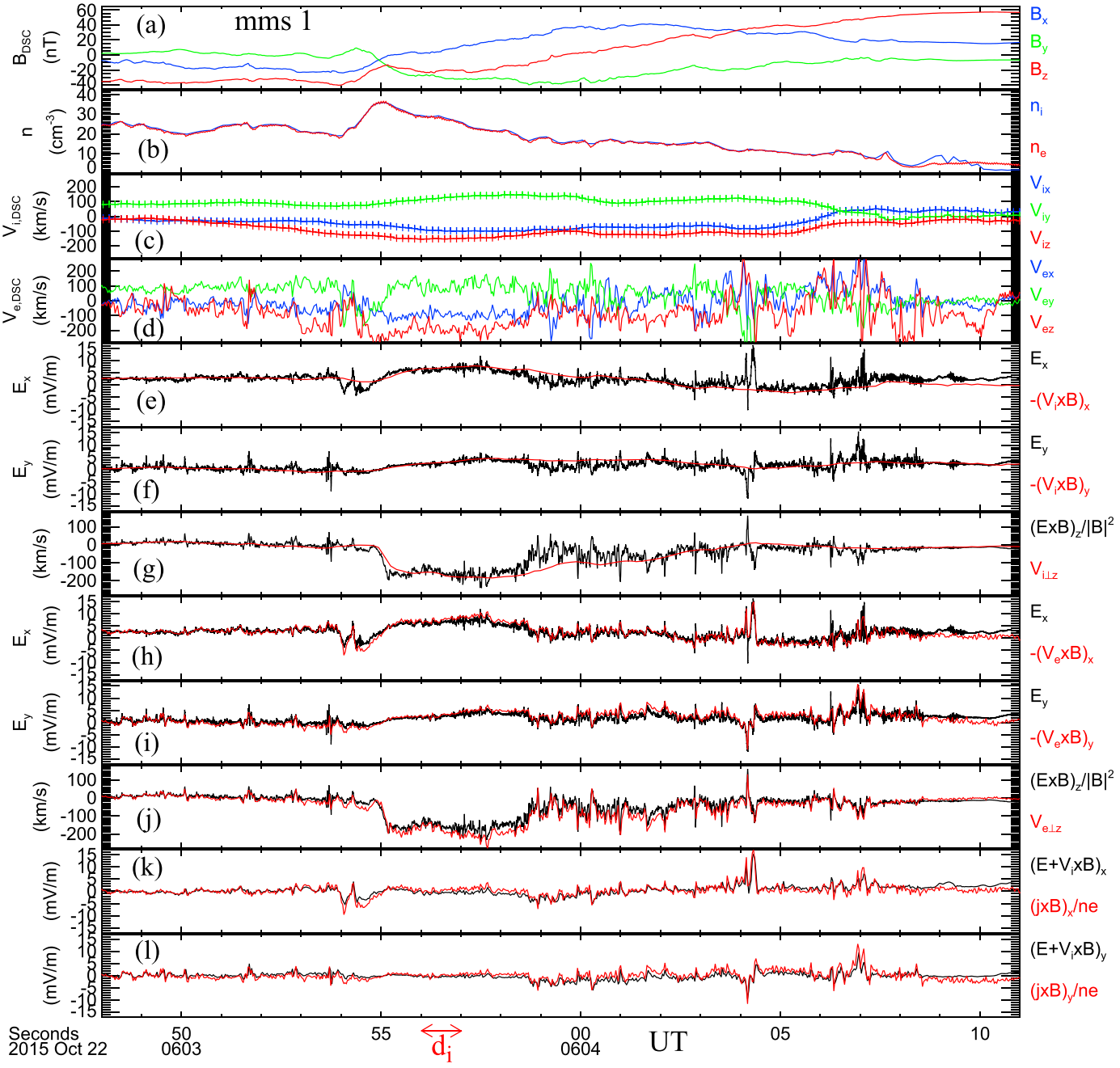

Figure 2. Ion and electron frozen-in conditions in the exhaust in despun spacecraft coordinate system (DSC), which is nearly identical to GSE. (a) Magnetic field, (b) ion and electron densities, (c and d) ion and electron velocities, (e and f) *x* and *y* components of the electric field and $-(\mathbf{v}_i \times \mathbf{B})$, (g) *z* component of the $\mathbf{E} \times \mathbf{B}$ velocity and perpendicular ion velocity, (h and i) *x* and *y* components of the electric field and $-(\mathbf{v}_e \times \mathbf{B})$, (j) *z* component of the $\mathbf{E} \times \mathbf{B}$ velocity and perpendicular electron velocity, and (k and l) *x* and *y* components of $(\mathbf{E} + \mathbf{v}_i \times \mathbf{B})$ and the Hall electric field $(\mathbf{j} \times \mathbf{B})/ne$. One-second duration corresponds to one d_i.

3. Current Layers in and Around the Reconnection Exhaust

Ions and electrons in an exhaust far downstream of the X line are thought to be mostly frozen-in. By evaluating the frozen-in conditions for ions $(\mathbf{E} + \mathbf{V}_i \times \mathbf{B} = 0)$ and electrons $(\mathbf{E} + \mathbf{V}_e \times \mathbf{B} = 0)$, one can evaluate the accuracy of the measurements. Further evaluation can be made by comparing the current density derived from plasma measurements and by the curlometer method.

3.1. Frozen-in Conditions for Ions and Electrons

We examine the frozen-in conditions in the despun spacecraft (DSC) coordinate system using the spin plane components of the electric field, E_x and E_y.

Figure 2 shows a zoom-in of the exhaust centered at ~06:04:00 UT (marked by the blue bar in Figure 1e). The difference between $\mathbf{V}_i$ (Figure 2c) and $\mathbf{V}_e$ (Figure 2d) traces is striking, with $\mathbf{V}_e$ being much more variable than $\mathbf{V}_i$ both in the exhaust and in the upstream magnetosheath. The good agreement, to within 1 mV/m in most regions, between $\mathbf{E}$ and $-\mathbf{V}_e\times\mathbf{B}$ in Figures 2h and 2i indicates that the electrons were frozen-in, as well as the high accuracy of the measurements of $\mathbf{V}_e$, $\mathbf{B}$, and $\mathbf{E}$. The 8192 samples per second electric field matches the lower resolution $-\mathbf{V}_e\times\mathbf{B}$ well, implying that there were essentially no electric field structures smaller than the d_e scale in this exhaust. A similar comparison between the z component of the perpendicular electron velocity and the $\mathbf{E}\times\mathbf{B}$ velocity (Figure 2j) reveals an agreement that is typically within 20 km/s in the magnetosheath and much of the magnetopause. There are regions (e.g., around the exhaust edge at 06:03:54–06:03:55 UT) where $E_x \neq (-\mathbf{V}_e\times\mathbf{B})_x$ (Figure 2h) which could indicate violation of the electron frozen-in condition there.

The ion frozen-in condition (Figures 2e and 2f), on the other hand, is violated in many parts of the exhaust and at its boundaries. While the violation within sub-d_i scale structures may not be surprising, it occurs in broader ion scale regions (e.g., 06:03:58.5–06:04:01.5 UT) as well, which is rather surprising.

Figures 2k and 2l show the comparison between $\mathbf{E}+\mathbf{V}_i\times\mathbf{B}$ and $\mathbf{j}\times\mathbf{B}$/ne (the Hall term in the generalized Ohm's law). The excellent agreement between the two quantities further illustrates the presence of Hall structures not only at the exhaust/current sheet boundaries but also within the exhaust and even in the magnetosheath, many of which are on electron scales.

3.2. Current Density From Plasma and Magnetic Field Measurements

The good agreement between $\mathbf{E}$ and $\mathbf{V}_e\times\mathbf{B}$ indicates that the electron velocity measurements are accurate (in addition to the electrons being frozen-in). On the other hand, ion and electron velocities often do not agree, implying the presence of currents. In this section we examine the current density derived from the plasma measurements, $\mathbf{j}_p$, and compare to the current density derived from the curlometer method, $\mathbf{j}_B$.

Figures 3d–3f overplot $\mathbf{j}_p$ for the four spacecraft and demonstrate that some large structures are coherent and stable (e.g., at the magnetosheath edge of the exhaust ~06:03:55 UT) and are seen by all four spacecraft as they traverse these current layers consecutively. Other current structures (e.g., at 06:04:04–06:04:04.5 UT) in the middle of the exhaust are less coherent. At the individual spacecraft, $\mathbf{j}_p$ is generally larger and has more structure than $\mathbf{j}_B$ (black traces in Figures 3g–3i). However, the "average" $\mathbf{j}_p$ at the four-spacecraft barycenter (red traces in Figures 3g–3i) is more similar to $\mathbf{j}_B$, which is also evaluated at the barycenter. This agreement serves as validations of $\mathbf{j}_p$ and $\mathbf{j}_B$. From this and the comparisons shown in Figure 2, we conclude that the plasma instruments provide accurate current density measurements at 30 ms, or 1.3 km (~d_e) resolution for this exhaust, which moved at 44 km/s relative to MMS.

3.3. Filamentary Currents and Vorticity in the Exhaust and at its Boundaries

The data reveal structure both at ion and electron scales. At the magnetosheath edge of the exhaust (at ~06:03:55 UT), a bipolar j_{PL} component was observed by all four spacecraft with amplitude up to 1 μA/m^2 (Figure 3d). An out-of-plane current j_{PM} of similar amplitude (Figure 3e) was observed concurrent with the bipolar j_{PL}. It took about 1 s to cross this current layer, which was on the order of 1 d_i. In addition to current flowing tangential to the magnetopause there was also a sunward directed normal current (j_{PN}) at this boundary (Figure 3f).

A bipolar j_{PL} was also observed by all four spacecraft at the magnetospheric edge of the exhaust (at 06:04:07 UT), but j_{PM} and j_{PN} were much weaker there (Figures 3d–3f).

The sense of j_{PL} located on the exhaust side of the boundaries is consistent with the positive B_M (Figure 3b) in the exhaust, but is opposite to the expected Hall current loop south of the X line for asymmetric reconnection.

In addition to the ion-scale bipolar currents at the boundaries of the exhaust, smaller-scale current layers were observed within the exhaust itself as well as in the adjacent magnetosheath. Some of these current densities have amplitudes comparable to those at the exhaust boundaries but are of smaller scales. An example is at 06:04:04–06:04:04.7 UT where the four spacecraft observed very different current density structures. MMS

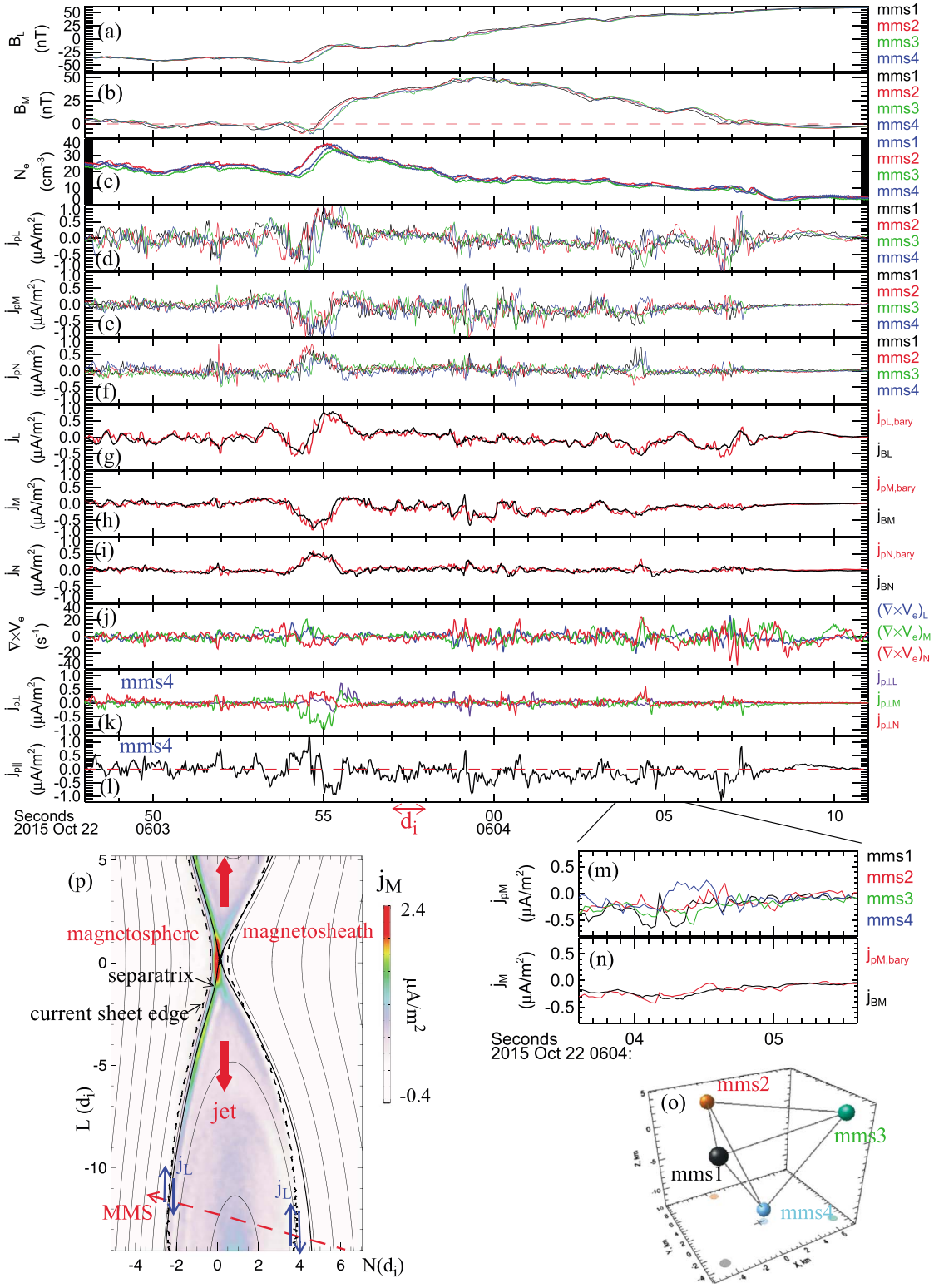

Figure 3. Filamentary currents in the exhaust and at its boundaries in LMN. (a and b) *L* and *M* components of magnetic field at MMS 1–4; (c) electron densities at MMS 1–4; (d–f) *L*, *M*, and *N* components of the current density computed from plasma measurements, j_P, at MMS 1–4; (g–i) *L*, *M*, and *N* components of the current density computed from $\nabla \times \mathbf{B}/\mu_0$ (black) and $\mathbf{j}_p$ at the four-spacecraft barycenter (red); (j) electron vorticity; (k and l) perpendicular and parallel components of $\mathbf{j}_p$ at MMS 4; (m) zoom-in of Figure 3e; (n) zoom-in of Figure 3h; (o) MMS tetrahedron; and (p) out-of-plane j_M and overall current sheet edges (dashed curves) from 2-D kinetic simulation using upstream conditions similar to the present MMS event, and rough sketches of spacecraft trajectory (red dashed arrow) and observed j_L directions (blue arrows) (see the supporting information section for details on the simulation setup and the method for identifying the current sheet edges).

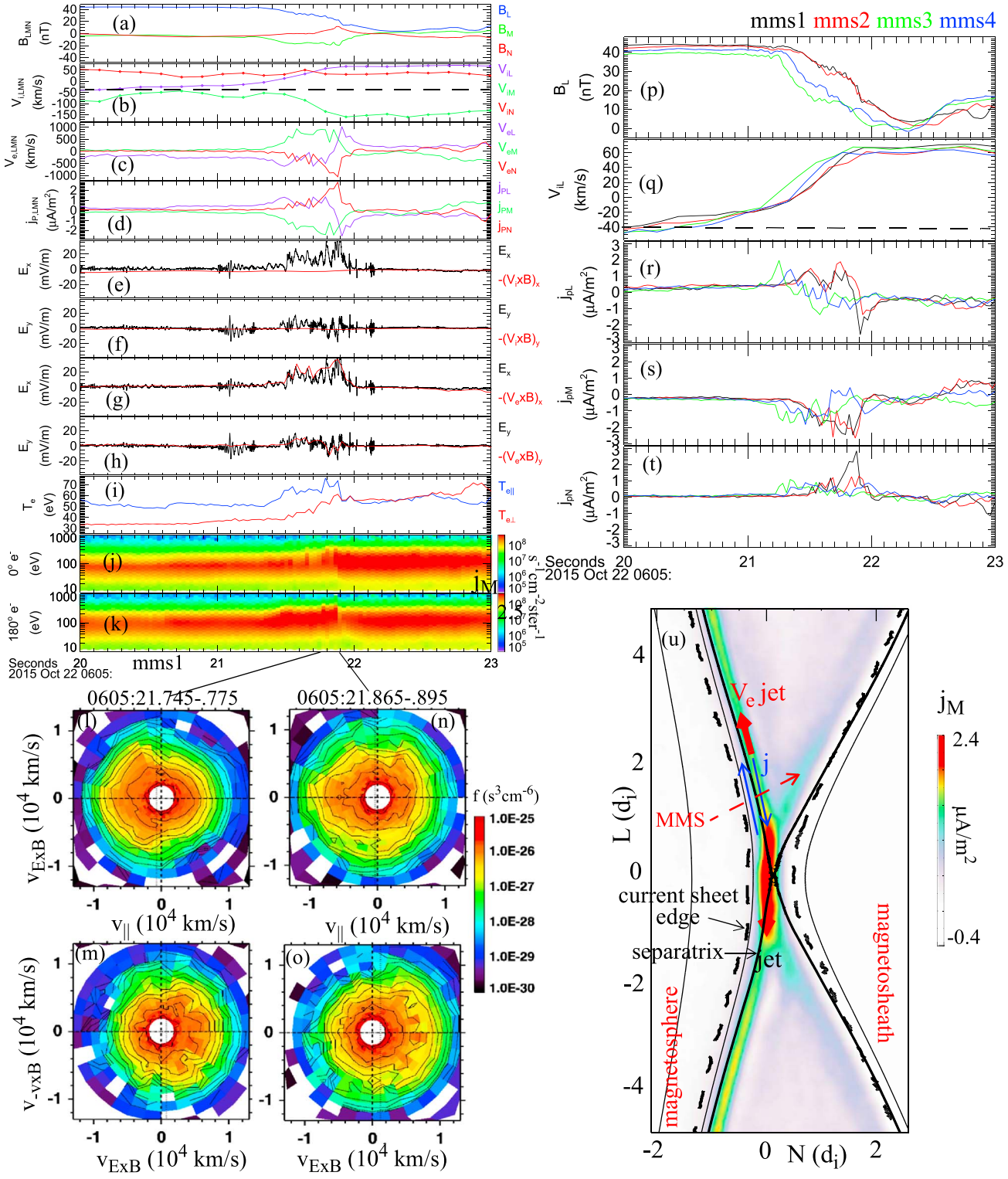

Figure 4. MMS 1 observations near the X line. (a) Magnetic field in LMN; (b and c) ion and electron velocities in LMN; (d) $\mathbf{j}_p$ in LMN; (e and f) *x* and *y* components of the electric field and $-(\mathbf{v}_i \times \mathbf{B})$ in DSC; (g and h) *x* and *y* components of the electric field and $-(\mathbf{v}_e \times \mathbf{B})$ in DSC; (i) electron temperature; (j and k) 0° and 180° pitch angle electron spectrograms in energy flux; (l and m) electron distribution sampled in the positive j_L layer in the $\mathbf{E} \times \mathbf{B}$ and $V_{||}$ plane, and in the $\mathbf{E} \times \mathbf{B}$ and $-\mathbf{v} \times \mathbf{B}$ plane; (n and o) same planes as Figures 4l and 4m but distributions sampled in the strong j_M layer; (p and q) B_L and V_L at MMS 1–4; (r–t) LMN components of $\mathbf{j}_p$ at MMS 1–4; and (u) j_M and overall current sheet edges (dashed curves) from 2-D kinetic simulation. Close to the X line, the separatrices are inward of the current sheet boundaries, whereas they are outside downstream. The crossover point occurs at $|L|$~3 d_i on the magnetosheath side and ~13d_i on the magnetospheric side (Figure 3p). This suggests that the length of the ion diffusion region may be asymmetric, longer on the magnetospheric side.

1 and MMS 4 observed opposite j_{PM} currents (up to 0.7 μA/m^2), while MMS 2 and 3 did not see much of a current (Figures 3m and 3n). With a spacecraft separation of 10 km, this implies that the spatial scale of this current layer was much less than 10 km. Differences between the measurements at the four spacecraft therefore reveal electron-scale filaments that persist throughout the exhaust crossing. These filamentary currents were Hall currents since electrons were frozen-in while the ions were not (Figure 2), and they had components both parallel and perpendicular to the magnetic field (Figures 3k and 3l).

Electron vortices (Figure 3j) were associated with the filamentary currents. The vorticity is larger in the exhaust than in the adjacent magnetosheath, suggesting that the vortices were generated by the reconnection process. Note that the four-spacecraft determination of $\nabla \times \mathbf{V}_e$ only measures vorticity at scale sizes larger than 10 km.

4. Intense and Filamentary Currents Close to the X line

We now examine the current structure around the ion flow reversal interval (marked by the red horizontal bar in Figure 1e), which occurred 80 s after the exhaust encounter, As pointed out in section 2, this near-X line region displayed stronger electron heating and more intense currents and electric fields than during the earlier exhaust encounter.

Figure 4d shows that the current structure consisted of a strong (up to 2.5 μA/m^2) out-of-plane current j_{PM}, approximately centered on the reversal of j_{PL}. Since $|V_e| \gg |V_i|$ (Figures 4b and 4c), this structure was dominated by electron currents. This current structure was observed by all four spacecraft (Figures 4r and 4s) as they approached the current sheet center ($B_L = 0$) from the $B_L > 0$ (magnetospheric) side. Since MMS 3 and 4 approached the overall current sheet center ahead of MMS 2 and 1 (Figure 4p), some of the time (e.g., 06:05:21.6–06:05:21.9 UT) MMS 3 and 4 detected negative j_{PL} while MMS 1,2 detected positive j_{PL}. This implies that the oppositely directed j_{PL} was a spatial feature. The negative j_{PL} was consistent with the Hall current north of the X line in asymmetric reconnection [e.g., *Tanaka et al.*, 2008]. Since the spacecraft separation was only ~10 km (~8 d_e), the filamentary j_{PL} currents must have had electron scale widths. The large negative j_{PL} ~2.5 μA/m^2 was associated with an outflowing electron jet (V_{eL}) with speed ~1000 km/s, which is ~4 times the hybrid Alfvén speed of the two inflow regions [*Cassak and Shay*, 2007] of 260 km/s.

The reversals of j_{PL} (Figure 4d) and V_{eL} (Figure 4c) at first seem to suggest that the spacecraft may have crossed the X line region, detecting bi-directional electron jets originating from the X line. However, this scenario is not consistent with the ion velocity measurements or the relative positions of the spacecraft. Figures 4a and 4b show that as the spacecraft approached the current sheet center, the ion outflow (V_{iL}) speed was already ~ +70 km/s (or 110 km/s relative to the magnetosheath V_{iL} of −40 km/s indicated by the horizontal dashed line in Figure 4b). In other words, the current structures were detected downstream (and north) of the X line. The spacecraft locations, with MMS 3 and 4 located sunward of MMS 1 and 2 (Figure 3o), together with the B_L variations (Figure 4p), reveal that the j_{PL} reversal (or layering) occurred in the magnetopause normal direction (Figure 4u). Furthermore, these electron currents were located deep inside the current sheet, where B_L~20–30 nT (compared to B_L~60 nT in the magnetosphere), instead of being at the edges of the current sheet (marked by the dashed curves in Figure 4u) as was the case far downstream of the X line.

Figures 4e and 4f show that there were significant structures in the electric field, with amplitudes up to ~40 mV/m in the electron current layer, in contrast to the much weaker fields at the exhaust boundaries far downstream of the X line. The ions were not frozen-in throughout the electron current layer (Figures 4e and 4f), while the electrons were mostly frozen-in, except perhaps in some substructures (Figures 4g and 4h).

Figure 4o shows that in the strong j_{PM} region, the electron distributions in the plane perpendicular to the magnetic field consisted of a mixture of nearly gyrotropic low-energy (magnetospheric) electrons and nongyrotropic (crescent shape) magnetosheath electrons at high energies/speeds (>5000 km/s) in the $\mathbf{E} \times \mathbf{B}$ direction.

Electron heating was associated with the electron current region (Figure 4i). Across this current region the perpendicular electron temperature increased by about 20 eV and remained at that level in the exhaust. The electron parallel temperature, on the other hand, started to increase before the perpendicular temperature rise, but was localized to the strong current region. Furthermore, Figures 4j–4l show that the parallel heating was associated with electrons flowing antiparallel to the magnetic field, which in this case (being north of the X line and on the magnetospheric side) corresponded to electrons flowing toward the X line.

5. Summary and Discussions

We have demonstrated that the MMS ion and electron moments were sufficiently accurate to provide unprecedented single-point current density measurements at 30 ms cadence (~d_e resolution), capable of resolving electron-scale current layers.

In the downstream exhaust region, filamentary Hall currents (in which the electrons were frozen-in but the ions were not) and electron vorticity were observed at the exhaust boundaries as well as within the exhaust itself. These currents have components both parallel and perpendicular to the magnetic field. Pairs of bipolar j_{PL} were seen at both edges of the exhaust. Electron-scale filamentary Hall currents embedded in reconnection exhausts have been seen in 3-D simulations [e.g., *Daughton et al*., 2014; *Nakamura and Daughton*, 2014] but appear to be less common in 2-D simulations. This suggests that these currents may be created by instabilities that are suppressed in 2-D. The ion flows in the exhaust were remarkably laminar and did not appear to be affected by the filamentary currents. The presence of Hall effects in the exhaust far downstream of the X line (and even in the magnetosheath) questions the identification of the ion diffusion region based on the violation of the ion-frozen-in condition alone.

Compared to the downstream exhaust region, the near-X line region exhibited more intense electron currents and electric fields, greater electron heating, and a super-Alfvénic outflowing electron jet. Another difference was an intense out-of-plane current flanked by bipolar j_{PL} located deep inside the current sheet, instead of being at the outer edges of the current sheet (marked by the dashed curves in Figures 3p and 4u) as was the case far downstream of the X line. In comparison with simulation (Figure 4u), the occurrence of intense j_{PM} and j_{PL} current structures deep inside the current sheet implies that MMS was within at most a few d_i from the X line. Close to the X line, such current structures are located right around the magnetospheric separatrix, inward of the exhaust/current sheet boundaries, and therefore embedded inside the ion diffusion region. In contrast, far downstream of the X line, the exhaust/current sheet boundaries are inward of the separatrices.

The near-X line electron current layer also exhibited nongyrotropic crescent shaped electron distributions that were similar to those predicted [*Hesse et al*., 2014; *Bessho et al*., 2016; *Shay et al*., 2016] and observed [*Burch et al*., 2016] in the immediate vicinity of the X line. These distributions are indicative of demagnetization and acceleration of electrons by the strong normal electric field (~E_x in Figure 4e), and their presence downstream of the X line is consistent with simulations [e.g., *Shay et al*., 2016]. Our finding could indicate that some electron physics around the X line extends downstream.

The observed current layers have some similarities but also significant differences with the expected Hall currents in the single X line reconnection picture. For asymmetric reconnection with inflow conditions similar to this event, one expects current to flow along the magnetospheric edge of the exhaust toward the X line and then along the magnetosheath edge away from the X line, creating a monopolar B_M in each exhaust [e.g., *Tanaka et al*., 2008; *Pritchett*, 2008]. Near the X line, the observed negative j_{PL} close to the current sheet center north of the X line was consistent with the Hall current direction. The associated super-Alfvénic electron jet located off the current sheet center on the magnetospheric side may be the asymmetric reconnection counterpart of the extended outflowing electron jet at the current sheet center in symmetric reconnection [*Shay et al*., 2007; *Karimabadi et al*., 2007; *Phan et al*., 2007].

At the exhaust 70 d_i downstream, the sense of j_{PL} located on the exhaust side, while consistent with the measured B_M, was opposite to the expected Hall current loop south of the X line. Another difference is the location of strong j_{PM}, which is predicted to be on the magnetospheric edge of the exhaust (Figure 3p), but was observed to be on the magnetosheath side instead. These discrepancies with the basic picture of asymmetric reconnection are puzzling and require further study.

Another feature of the MMS observations that is not apparent in kinetic simulations was the presence of narrow j_{PL} upstream of exhaust boundaries. Such narrow currents are seen in simulations of symmetric reconnection but are generally not seen in asymmetric reconnection simulations. These and other puzzles will emerge as we explore the unprecedented plasma and field measurements made by MMS.

Acknowledgments
Research supported by NSF grants AGS-1103303 and AGS-0953463 and NASA grants NNX13AD72G, NNX08AO83G, NNX08A084G, NNX16AF75G, and NNX16AG76G. Data source: MMS Science Data Center at lasp.colorado.edu/mms/sdc/public/. J.P.E was supported by STFC(UK) grants ST/K001051/1 and ST/N000692/1.

References

Bessho, N., L.-J. Chen, and M. Hesse (2016), Electron distribution functions in the diffusion region of asymmetric magnetic reconnection, *Geophys. Res. Lett.*, *43*, 1828–1836, doi:10.1002/2016GL067886.
Burch, J. L., et al. (2016), Electron-scale measurements of magnetic reconnection in space, *Science*, doi:10.1126/science.aaf2939.

Cassak, P. A., and M. A. Shay (2007), Scaling of asymmetric magnetic reconnection: General theory and collisional simulations, *Phys. Plasmas*, *14*, 102114, doi:10.1063/1.2795630.

Che, H., J. F. Drake, and M. Swisdak (2011), A current filamentation mechanism for breaking magnetic field lines during reconnection, *Nature*, *474*, 184–187, doi:10.1038/nature10091.

Cowley, S. W. H. (1982), The causes of convection in the Earth's magnetosphere - A review of developments during the IMS, *Rev. Geophys. Space Phys.*, *20*, 531, doi:10.1029/RG020i003p00531.

Daughton, W., V. Roytershteyn, H. Karimabadi, L. Yin, B. J. Albright, B. Bergen, and K. J. Bowers (2011), Role of electron physics in the development of turbulent magnetic reconnection in collisionless plasmas, *Nat. Phys.*, *7*, 539–542, doi:10.1038/nphys1965.

Daughton, W., T. K. M. Nakamura, H. Karimabadi, V. Roytershteyn, and B. Loring (2014), Computing the reconnection rate in turbulent kinetic layers by using electron mixing to identify topology, *Phys. Plasmas*, *21*, 052307, doi:10.1063/1.4875730.

Dunlop, M. W., A. Balogh, K.-H. Glassmeier, and P. Robert (2002), Four-point Cluster application of magnetic field analysis tools: The curlometer, *J. Geophys. Res.*, *107*(A11), 1384, doi:10.1029/2001JA0050088.

Fuselier, S. A., D. M. Klumpar, and E. G. Shelley (1990), Ion reflection and transmission during reconnection at the Earth's subsolar magnetopause, *Geophys. Res. Lett.*, *18*(2), 139–142, doi:10.1029/90GL02676.

Gosling, J. T., M. F. Thomsen, S. J. Bame, R. C. Elphic, and C. T. Russell (1991), Observations of reconnection of interplanetary and lobe magnetic field lines at the high-latitude magnetopause, *J. Geophys. Res.*, *96*, 14,097–14,106, doi:10.1029/91JA01139.

Hesse, M., N. Aunai, D. Sibeck, and J. Birn (2014), On the electron diffusion region in planar, asymmetric, systems, *Geophys. Res. Lett.*, *41*, 8673–8680, doi:10.1002/2014GL061586.

Karimabadi, H., W. Daughton, and J. Scudder (2007), Multi-scale structure of the electron diffusion region, *Geophys. Res. Lett.*, *34*, L13104, doi:10.1029/2007GL030306.

Krauss-Varban, D., H. Karimabadi, and N. Omidi (1999), Two-dimensional structure of the co-planar and non-coplanar magnetopause during reconnection, *Geophys. Res. Lett.*, *26*, 1235–1238, doi:10.1029/1999GL900211.

Nakamura, T. K. M., and W. Daughton (2014), Turbulent plasma transport across the Earth's low-latitude boundary layer, *Geophys. Res. Lett.*, *41*, 8704–8712, doi:10.1002/2014GL061952.

Phan, T. D., J. F. Drake, M. A. Shay, F. S. Mozer, and J. P. Eastwood (2007), Evidence for an elongated (>60 ion skin depths) electron diffusion region during fast magnetic reconnection, *Phys. Rev. Lett.*, *99*, 255002, doi:10.1103/PhysRevLett.99.255002.

Pollock, C., et al. (2016), Fast plasma investigation for Magnetospheric Multiscale, *Space Sci. Rev.*, doi:10.1007/s11214-016-0245-4.

Pritchett, P. L. (2008), Collisionless magnetic reconnection in an asymmetric current sheet, *J. Geophys. Res.*, *113*, A06210, doi:10.1029/2007JA012930.

Robert, P., M. W. Dunlop, A. Roux, and G. Chanteur (1998), Accuracy of current density determination, in *Analysis Methods for Multi-Spacecraft Data*, edited by G. Paschmann and P. W. Daly, pp. 395–418, International Space Science Institute, Bern.

Russell, C. T., et al. (2014), The Magnetospheric Multiscale Magnetometers, *Space Sci. Rev.*, 1–68, doi:10.1007/s11214-014-0057-3.

Shay, M. A., J. F. Drake, and M. Swisdak (2007), Two-scale structure of the electron dissipation region during collisionless magnetic reconnection, *Phys. Rev. Lett.*, *99*, 155002, doi:10.1103/PhysRevLett.99.155002.

Shay, M. A., T. D. Phan, C. C. Haggerty, M. Fujimoto, J. F. Drake, K. Malakit, P. A. Cassak, and M. Swisdak (2016), Kinetic signatures of the region surrounding the X-line in asymmetric (magnetopause) reconnection, *Geophys. Res. Lett.*, *43*, 4145–4154, doi:10.1002/2016GL069034.

Sonnerup, B. U. Ö. (1979), Magnetic field reconnection, in *Solar System Plasma Physics*, vol. 3, edited by L. J. Lanzerotti, C. F. Kennel, and E. N. Parker, pp. 46, North Halland Pub, Amsterdam.

Sonnerup, B. U. Ö., and L. J. Cahill Jr. (1967), Magnetopause structure and attitude from Explorer 12 observations, *J. Geophys. Res.*, *72*(1), 171–183, doi:10.1029/JZ072i001p00171.

Swisdak, M., J. F. Drake, M. A. Shay, and J. G. McIlhargey (2005), Transition from antiparallel to component magnetic reconnection, *J. Geophys. Res.*, *110*, A05210, doi:10.1029/2004JA010748.

Tanaka, K. G., et al. (2008), Effects on magnetic reconnection of a density asymmetry across the current sheet, *Ann. Geophys.*, *26*, 2471–2483, doi:10.5194/angeo-26-2471-2008.

Tanaka, K., M. Fujimoto, and I. Shinohara (2010), Physics of magnetopause reconnection: A study of the combined effects of density asymmetry, velocity shear, and guide field, *Int. J. Geophys.*, *2010*, 202583, doi:10.1155/2010/202583.

Torbert, R. B., et al. (2014), The FIELDS instrument suite on MMS: Scientific objectives, measurements, and data products, *Space Sci. Rev.*, doi:10.1007/s11214-014-0109-8.